



OPEN

Antiferromagnetic FeSe monolayer on SrTiO₃: The charge doping and electric field effects

SUBJECT AREAS:

SUPERCONDUCTING
PROPERTIES AND
MATERIALSSURFACES, INTERFACES AND
THIN FILMSMAGNETIC PROPERTIES AND
MATERIALSELECTRONIC PROPERTIES AND
MATERIALSFawei Zheng^{1,2}, Zhigang Wang^{1,2}, Wei Kang³ & Ping Zhang^{1,2,3}¹LCP, Institute of Applied Physics and Computational Mathematics, Beijing 100088, People's Republic of China, ²Beijing Computational Science Research Center, Beijing 100084, People's Republic of China, ³Center for Applied Physics and Technology, Peking University, Beijing 100871, People's Republic of China.Received
18 April 2013Accepted
1 July 2013Published
18 July 2013Correspondence and
requests for materials
should be addressed to
P.Z. (zhang_ping@
iapcm.ac.cn)

By growing monolayer FeSe on SrTiO₃(001) surface, researchers obtain the highest superconducting transition-temperature for iron-based superconductor. Here, we study the antiferromagnetic (AFM) checkerboard monolayer FeSe adsorbed on SrTiO₃(001) surface. We show that the system has a considerable charge transfer from SrTiO₃(001) substrate to FeSe monolayer, and so has a self-constructed electric field. The FeSe monolayer band structure near the Brillouin zone (BZ) center is sensitive to charge doping, and the spin-resolved energy bands at BZ corner are distorted to be flattened by the perpendicular electric field. It is revealed that the striking disappearance of the Fermi surface around the BZ center can be well explained by the AFM checkerboard phase with charge doping and electric field effects. We propose a tight-binding model Hamiltonian to take these key factors into account. We also show that this composite structure is an ideal electron-hole bilayer system, with electrons and holes respectively formed in FeSe monolayer and TiO₂ surface layer.

Due to its simple crystal structure, prominent antiferromagnetic magnetic ordering, and significant pressure effect on superconductivity, during the last few years FeSe binary superconductor has been drawing extensive attention from fundamental mechanism of Fe-based superconductivity to promising application in such areas as superconducting wires and thin films¹. Recently, monolayer FeSe with atomic flatness was successfully grown on SrTiO₃(001) surface², and strikingly, the high-temperature superconductivity signature from the monolayer was revealed by high energy resolution scanning tunneling spectroscopy (STS). It is even hopeful that with further improving the sample quality, the transition temperature is probably as high as 77 K, the liquid nitrogen boiling point. The subsequent angle-resolved photoemission spectroscopy (ARPES) experiment³ shows that the Fermi surface of this FeSe monolayer only consists of electron pockets near the Brillouin zone (BZ) corner, with no hole pockets around the zone center observed. The $T_c = 65 \pm 5$ K is realized by optimizing the annealing process⁴, and spin density wave is also identified in FeSe/SrTiO₃ thin films⁵. Theoretical efforts are being paid to explain these intriguing STS and ARPES reports. The soft phonon of SrTiO₃(001) was found to strengthen the Cooper pairing⁶. S_4 symmetry was also noticed⁷, wherein it was suggested that cuprates and iron-based superconductors share an identical high- T_c superconducting mechanism. The density functional theory (DFT) total-energy calculations gave that collinear antiferromagnetic order (CAFM) FeSe monolayer on TiO₂ terminated SrTiO₃(001) surface is the most stable structure, and there is neither hybridization nor charge transfer between FeSe monolayer and SrTiO₃(001) surface⁸. The calculated Fermi surface for this CAFM structure exists around the M point in the folded BZ, and there is a Dirac-cone-like bands of FeSe near Fermi energy, which unfortunately are not observed by the ARPES measurement³ that the Fermi surface disappears around the zone center. A more recent DFT study⁹ on a single FeSe monolayer (without substrate) showed that an AFM checkerboard phase (we will use AFM for simplicity in the following texts) instead of CAFM phase can have the Fermi surface resembling the ARPES data. Basically, however, the interaction between AFM-ordered FeSe monolayer and SrTiO₃(001) surface remains largely unclear in literature, despite its urgent importance on understanding the key role played by the interface in controlling the Fermi surface topology and high-temperature superconductivity of FeSe monolayer.

In this work, we carefully investigate with DFT based *ab initio* calculations the electronic structure of AFM FeSe monolayer on TiO₂ terminated SrTiO₃(001) surface. We show that the calculated electronic structure of the system is close to the ARPES experimental results. The charge transfer and electric field are induced by the

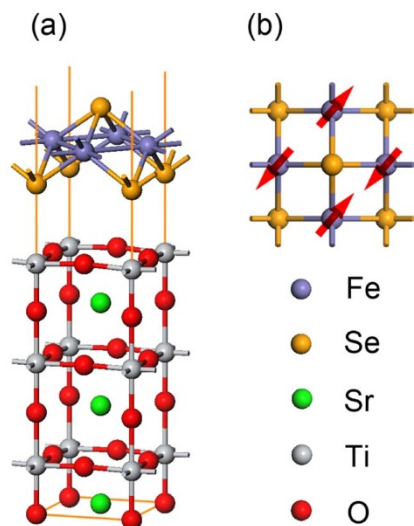


Figure 1 | The side view (a) and top view (b) for the atomic structure of monolayer FeSe adsorbed on TiO_2 terminated $\text{SrTiO}_3(001)$ surface. The magnetic ordering is also represented in top view (b) as red arrows.

interaction between $\text{SrTiO}_3(001)$ substrate and AFM FeSe monolayer, and turn back out to play an important role in modulating the band structure and Fermi-surface topology of the FeSe monolayer. One extraordinary consequence is that the spin-resolved electron pockets surrounding the BZ corner are distorted and become flattened. We propose a tight-binding model Hamiltonian that can describe these key factors.

Results

We use 6-layer $\text{SrTiO}_3(001)$ slabs to mimic the surface of SrTiO_3 substrate, as shown in Fig. 1(a). The $\text{SrTiO}_3(001)$ surface is either SrO or TiO_2 terminated with nearly the same surface energy^{10–12}. According to the experiment², we use the TiO_2 terminated surface in our atomic models. FeSe monolayer is adsorbed on the 1×1 two-dimensional unit cell of TiO_2 -terminated $\text{SrTiO}_3(001)$ surface. To test the influence of SrTiO_3 antiferrodistortion on surface electronic structures, we also calculated a $\sqrt{2} \times \sqrt{2}$ supercell, in which the lower four layers of TiO_2 and SrO are fixed to their bulk positions and the octahedral rotation angle is set to the experimental value 2.1° ¹³. In our models, the vacuum space is larger than 10 \AA . The results are also checked for vacuum space larger than 20 \AA . The bulk calculation shows that the lattice parameter of SrTiO_3 is 3.901 \AA , which agrees well with experiments and previous theoretical results. The adsorption structure relaxation is performed with fixed lattice parameter of 3.901 \AA .

The relaxed adsorption structure of FeSe monolayer on TiO_2 terminated $\text{SrTiO}_3(001)$ surface is shown in Fig. 1. The lower layer Se atoms are on the top of Ti atoms, while the Fe atoms locate on the top of O atoms. The vertical distance between Ti and Se atoms is 3.13 \AA , which is slightly larger than that of the CAFM phase by 0.07 \AA . The vertical distance between Fe and O atoms is 4.43 \AA . The O atoms in the TiO_2 top-layer arise slightly, they are 0.1 \AA higher than Ti atoms. The distance between top (bottom) Se atoms and the Fe plane is 1.41 (1.40) \AA , and the Fe-Se-Fe angle for top (bottom) Se atoms is 108.5 (108.7) degrees. The magnetic moment on each atom is calculated by integrating the spin density in Wigner-Seitz radius of 1.30 \AA , 1.16 \AA , 2.14 \AA , 1.22 \AA , and 0.82 \AA for Fe, Se, Sr, Ti, and O atoms respectively. The calculated magnetic moment is $2.4 \mu_B$ on each Fe atom and is negligible on the other atoms.

The energy bands for spin-up channel are shown in Fig. 2(a). The spin-down energy bands are the same as those for spin-up channel except for an exchange of X and X' points in BZ. There are two bands

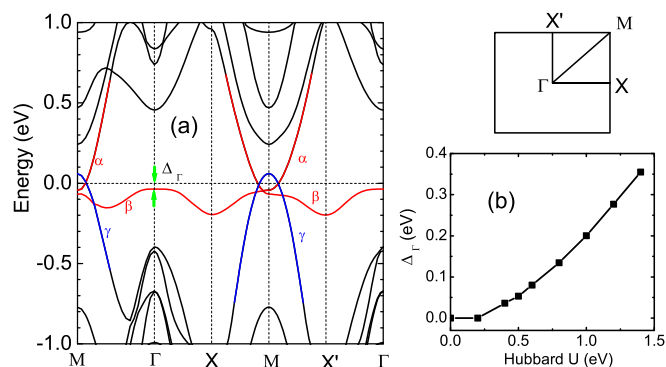


Figure 2 | The spin-up energy bands of monolayer FeSe adsorbed on TiO_2 terminated $\text{SrTiO}_3(001)$ surface (a). The red and blue lines are contributed by $3d$ orbitals on Fe atoms and $2p$ orbitals on O atoms, respectively. The Fermi level is set to be zero. Panel (b) shows the influence of Hubbard- U on the energy difference Δ_Γ .

[indicated as α and γ in Fig. 2(a)] crossing the Fermi level E_F near M point and forming an ideal pair of electron-hole bands with perfect Fermi-surface nesting, while around Γ point no metallic bands occur. Thus, the calculated Fermi surface only exists at the BZ corner, which agrees with the ARPES result in experiment³. In our calculations, the antiferrodistortion of SrTiO_3 substrate does not have considerable influence to the electronic structure of adsorbed AFM FeSe monolayer.

The disappearance of Fermi surface at BZ center is the result of a full electron filling of band β . We find that the shape of band β can be altered dramatically by changing the value of Hubbard- U correction. Actually, band β shall cross the Fermi level at the BZ center in the absence of Hubbard- U correction. When the Hubbard- U correction is applied, band β lowers its energy and a gap of 41 meV [indicated by green arrows in Fig. 2(a)] is obtained for $U = 0.5 \text{ eV}$, which agrees with the experimental result³. The detailed relationship between the minimum energy difference of band β and E_F around the BZ center (denoted as Δ_Γ) and the Hubbard- U correction is shown in Fig. 2(b). One can see that Δ_Γ and U are mainly in a linear relation. We have checked that this phenomenon does not exist in the paramagnetic FeSe/ SrTiO_3 system, wherein there are energy bands crossing the Fermi level around the BZ center even for 5.0 eV Hubbard- U correction.

Our PDOS (partial density of states) analysis shows that bands α and β are contributed by Fe $3d$ orbitals, while the hole-type band γ comes from the O $2p$ orbitals. We analyze the wavefunctions of band β at Γ point and bands α , β and γ at M point. The wavefunction of band β at Γ point shows a shape of a dumbbell in z -direction with a torus in xy -plane, which is the typical d_{z^2} feature. Whereas, the wavefunctions of bands α and β at M point show vertical four-leaf shapes, which are the d_{xz} and d_{yz} features. The wavefunctions for band γ are dumbbell shaped p_x and p_y orbitals that are mainly distributed on the surface O atoms. The crossing between bands α and γ indicates that charge transfer occurs from surface O atoms of SrTiO_3 substrate to Fe atoms of FeSe monolayer. Our Bader analysis identifies a charge transfer of $-0.17 e$ per unit cell.

Discussion

From the above results, we know that the AFM FeSe monolayer is charge doped by the SrTiO_3 substrate. In order to analyze this effect, we study a free-standing AFM FeSe monolayer by doping charge from $-0.5 e$ to $0.5 e$. The results are shown in Fig. 3. We see that the shape of band β changes dramatically when the system is positively charged. Band β at Γ point crosses the Fermi level, and becomes a hole pocket. When the FeSe monolayer is negatively charged, the shape of band β keeps static, while band α at Γ point

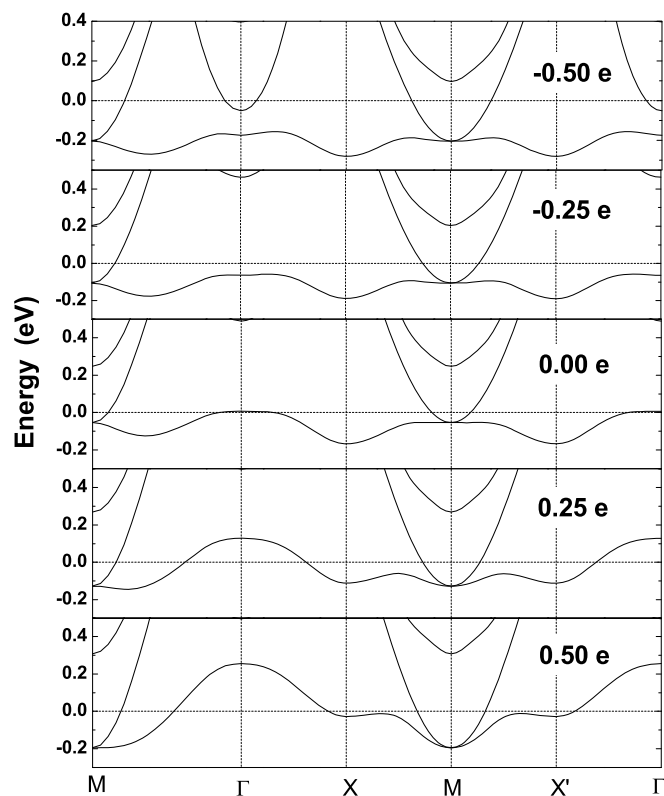


Figure 3 | The electronic energy bands of free-standing monolayer FeSe with 0.5 eV Hubbard- U correction and different levels of charge doping. The value of charge doping is changed from $-0.5 e$ to $0.5 e$ per unit cell. The Fermi energy is set to zero.

lowers its energy and finally crosses the Fermi energy, showing an electron pocket. Both positive and negative charge doping increase E_F relative to the energy of band α and β at M point. These results agree well with the previous study on FeSe monolayer without Hubbard- U correction⁹. However, as we have determined above, the realistic charge transfer in FeSe/SrTiO₃ is only $-0.17e$. By comparison with Fig. 3, we find that this value is not large enough for the existence of electron pocket at Γ point. Thus, the energy bands of AFM FeSe monolayer are altered limitedly by pure charge doping from SrTiO₃ substrate.

Besides the charge doping, another prominent feature in Fig. 2 is that bands α and β are nonsymmetric along M-X and M-X' directions, and a small splitting appears at M point. Whereas, for the free-standing AFM FeSe monolayer, bands α and β are symmetric along M-X and M-X' directions, and they are degenerate at M point for both neutral and charged systems as shown in Fig. 3. Considering the net charge and dipole effect of SrTiO₃ substrate, a vertical electric field may exist in FeSe/SrTiO₃. Then we further study the electric field effect. In our further DFT calculations, a free-standing monolayer FeSe is particularly designed to be exposed in a perpendicular electric field, and the atomic positions are relaxed for each electric field strength. The calculation results are shown in Fig. 4. Clearly, when the electric field strength is zero, the energy bands are symmetric along M-X and M-X' directions, and the bands of spin-up and spin-down components are the same. When the electric field strength is nonzero, however, we are astonished to see that the energy bands along M-X and M-X' directions become nonsymmetric, with an obvious spin splitting at M point. The splitting amplitude increases with increasing the electric field strength. So we verify that the energy bands near the Fermi energy and M point are distorted by the perpendicular electric field, and the energy of band α at X and X' points are different. Besides that, the features of spin-up and

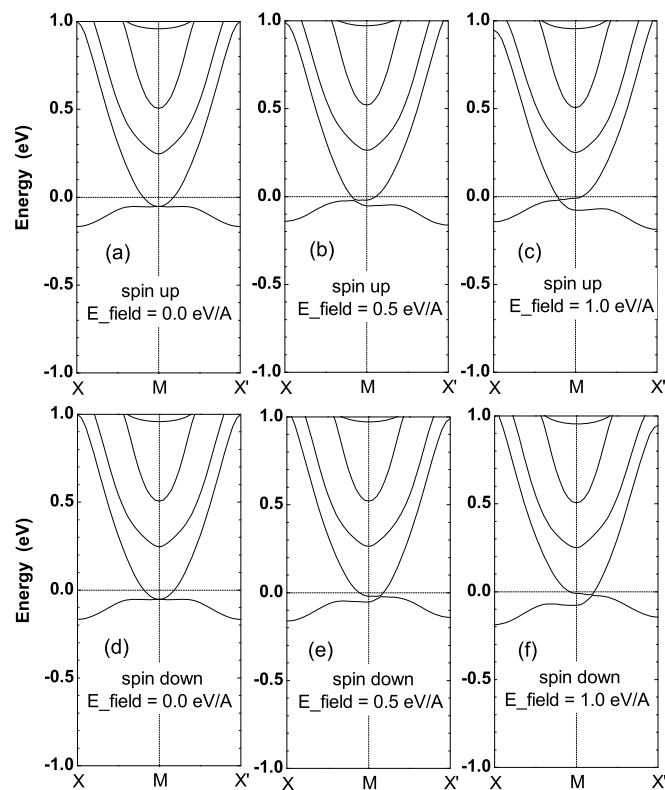


Figure 4 | The electronic energy bands of free-standing monolayer FeSe with different vertical electric field strength. The value of electric field strength is changed from 0.0 eV/\AA to 1.0 eV/\AA . The energy bands near Fermi energy are distorted and show different behaviors for spin-up and spin-down channels. The Fermi energy is set to zero.

spin-down bands are just opposite, namely, the energy bands in M-X' (M-X) direction for spin-up electrons are just the same as the energy bands in M-X (M-X') direction for spin-down electrons. Comparing the spin-up bands in Fig. 4 for free-standing FeSe monolayer and those for FeSe monolayer on SrTiO₃ surface (Fig. 2), we see that the distortion of the energy bands are quite similar. Moreover, the FeSe monolayer energy bands near M point along Γ -M direction shows an energy gap of $\sim 30 \text{ meV}$ when the applied electric field is 0.5 eV/\AA , which agrees well with Fig. 3(i) and 3(j) in Ref. 4. Thus, the effect of self-established electric field in FeSe/SrTiO₃ is confirmed.

To explore the detailed mechanism of energy band distortion, we construct a tight-binding model Hamiltonian to describe the system. As we have discussed above, the corresponding wavefunctions of bands α and β near M point are composed of d_{xz} and d_{yz} orbitals of Fe atom, and the wavefunction of energy band β near Γ point mainly comes from d_{z^2} orbital of Fe atom. From Fig. 4 we know that the energy band distortion mainly occurs near M point. Thus, we will use d_{xz} and d_{yz} orbitals of Fe atoms in our tight-binding model, and neglect the d_{z^2} orbital for simplicity. However, the vertical electric field could not affect a model which only consists of d_{xz} and d_{yz} orbitals of Fe atoms, since all the centers of these orbitals are in a horizontal plane. Thus some out-plane orbitals should be included in our model. The most natural choice is to use the orbitals of top and bottom Se atoms. We assume the Se orbitals in our model are symmetric in xy -plane, which may be Se $4p_z$ orbital or its combination with Se $4s$ orbital. The following calculation shows that this assumption well describes the energy bands along M-X and M-X' directions.

In our mean-field tight-binding model of AFM FeSe monolayer, we describe the spin-up and spin-down electrons separately. For spin-up electrons, the tight-binding model contains d_{xz} and d_{yz} orbitals of the spin-up Fe atom, besides one symmetric orbital for each Se

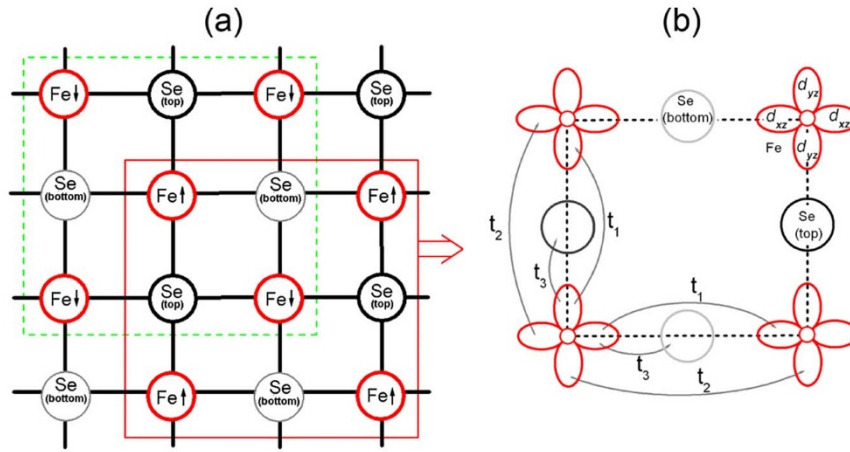


Figure 5 | (a) Atomic structure of FeSe monolayer. The red rectangle and green dash rectangle show two unit cells of AFM FeSe monolayer. Panel (b) shows the hopping schematic diagram of spin-up tight-binding model in a unit cell. The red, black, and gray circles show the positions of Fe atoms, top Se atoms and bottom Se atoms separately. In panel (b) the spin-down Fe atom is located at the cell center and is not plotted in this spin-up tight-binding model. The spin-down tight-binding model can be obtained by rotating panel (b) with 90 degrees or exchanging the positions of black and gray circles.

atom. Similarly, for spin-down electrons, the tight-binding model contains d_{xz} and d_{yz} orbitals of the spin-down Fe atom, and one symmetric orbital for each Se atom. The hopping of spin-up electrons is schematically shown in Fig. 5. For spin-down electrons, whereas, the hopping schematic diagram can be obtained by switching the positions of top and bottom Se atoms.

Considering the symmetry of each orbital, the tight-binding model Hamiltonian for spin-up electrons is written as $H^{(\text{up})} = H_{\text{on-site}}^{(\text{up})} + H_T^{(\text{up})}$, where $H_{\text{on-site}}^{(\text{up})}$ and $H_T^{(\text{up})}$ are shown in Eqs. (1) and (2) respectively. In these equations, $c_{xz,\vec{r}}^+$ and $c_{yz,\vec{r}}^+$ are creation operators of Fe d_{xz} and d_{yz} orbitals, while $c_{\text{top},\vec{r}}^+$ and $c_{\text{bot},\vec{r}}^+$ are those of top and bottom Se symmetric orbitals, respectively. For simplicity the spin indices are omitted. The parameter d is the distance

$$H_{\text{on-site}}^{(\text{up})} = \sum_{\vec{r}} \left[\epsilon_d \left(c_{xz,\vec{r}}^+ c_{xz,\vec{r}} + c_{yz,\vec{r}}^+ c_{yz,\vec{r}} \right) + (\epsilon_s + dE) c_{\text{top},\vec{r}}^+ c_{\text{top},\vec{r}} + (\epsilon_s - dE) c_{\text{bot},\vec{r}}^+ c_{\text{bot},\vec{r}} \right]. \quad (1)$$

$$H_T^{(\text{up})} = \sum_{\vec{r}} \left[t_1 \left(c_{yz,\vec{r}}^+ c_{yz,\vec{r}+\hat{y}} + c_{xz,\vec{r}}^+ c_{xz,\vec{r}+\hat{x}} \right) + t_2 \left(c_{xz,\vec{r}}^+ c_{xz,\vec{r}+\hat{y}} + c_{yz,\vec{r}}^+ c_{yz,\vec{r}+\hat{x}} \right) + t_3 \left(c_{xz,\vec{r}}^+ c_{\text{bot},\vec{r}+\hat{x}/2} + c_{yz,\vec{r}}^+ c_{\text{top},\vec{r}+\hat{y}/2} \right) \right] + h.c. \quad (2)$$

$$H_{\text{on-site}}^{(\text{down})} = \sum_{\vec{r}} \left[\epsilon_d \left(c_{xz,\vec{r}}^+ c_{xz,\vec{r}} + c_{yz,\vec{r}}^+ c_{yz,\vec{r}} \right) + (\epsilon_s + dE) c_{\text{top},\vec{r}}^+ c_{\text{top},\vec{r}} + (\epsilon_s - dE) c_{\text{bot},\vec{r}}^+ c_{\text{bot},\vec{r}} \right]. \quad (3)$$

$$H_T^{(\text{down})} = \sum_{\vec{r}} \left[t_1 \left(c_{yz,\vec{r}}^+ c_{yz,\vec{r}+\hat{y}} + c_{xz,\vec{r}}^+ c_{xz,\vec{r}+\hat{x}} \right) + t_2 \left(c_{xz,\vec{r}}^+ c_{xz,\vec{r}+\hat{y}} + c_{yz,\vec{r}}^+ c_{yz,\vec{r}+\hat{x}} \right) + t_3 \left(c_{xz,\vec{r}}^+ c_{\text{top},\vec{r}+\hat{x}/2} + c_{yz,\vec{r}}^+ c_{\text{bot},\vec{r}+\hat{y}/2} \right) \right] + h.c. \quad (4)$$

between top (or bottom) Se atom and Fe plane, and E are the electric field strength.

The tight-binding model Hamiltonian for spin-down electrons is similar to that of spin-up electrons, except for that the positions of

top and bottom Se atoms are exchanged. Thus, the Hamiltonian for spin-down electrons is written as $H^{(\text{down})} = H_{\text{on-site}}^{(\text{down})} + H_T^{(\text{down})}$, where $H_{\text{on-site}}^{(\text{down})}$ and $H_T^{(\text{down})}$ are shown in equation (3) and (4) respectively.

By performing the Fourier transformation, the model Hamiltonians for spin-up and spin-down electrons in momentum space are given by Eqs. (5) and (6),

$$H^{(\text{up})}(\mathbf{k}) = \begin{bmatrix} \epsilon_{d_x}(\mathbf{k}) & 0 & -it_3 \sin(k_y/2) & 0 \\ 0 & \epsilon_{d_z}(\mathbf{k}) & 0 & -it_3 \sin(k_x/2) \\ it_3 \sin(k_y/2) & 0 & \epsilon_{\text{top}} & 0 \\ 0 & it_3 \sin(k_x/2) & 0 & \epsilon_{\text{bot}} \end{bmatrix}, \quad (5)$$

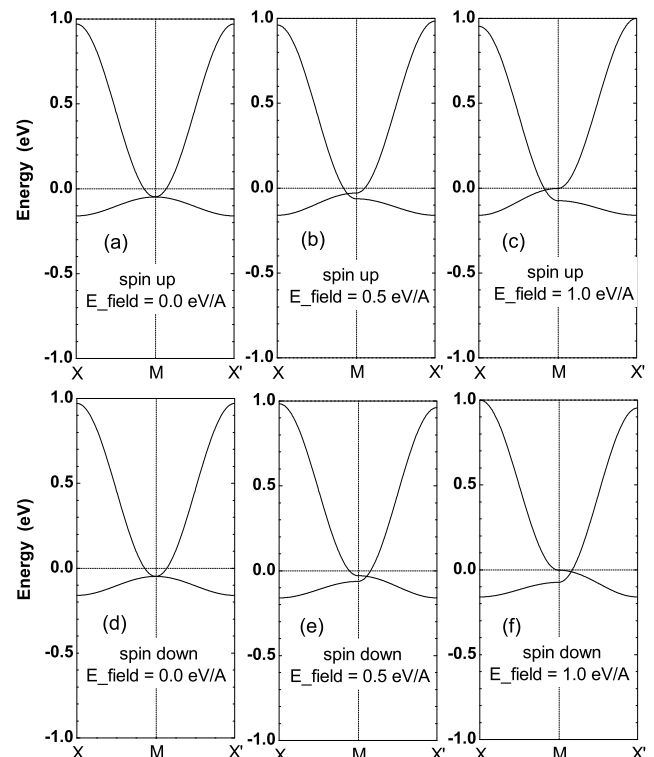


Figure 6 | Calculated tight-binding energy bands of monolayer FeSe for spin-up (a–c) and spin-down (d–f) channels. The energy bands distortion is shown near M point. The Fermi energy is set to zero.



$$H^{(\text{down})}(\mathbf{k}) = \begin{bmatrix} \epsilon_{d_{xz}}(\mathbf{k}) & 0 & -it_3 \sin(k_x/2) & 0 \\ 0 & \epsilon_{d_{yz}}(\mathbf{k}) & 0 & -it_3 \sin(k_y/2) \\ it_3 \sin(k_x/2) & 0 & \epsilon_{\text{top}} & 0 \\ 0 & it_3 \sin(k_y/2) & 0 & \epsilon_{\text{bot}} \end{bmatrix}, \quad (6)$$

where $\epsilon_{d_{xz}}(\mathbf{k}) = \epsilon_d + t_1 \cos(k_y) + t_2 \cos(k_x)$, $\epsilon_{d_{yz}}(\mathbf{k}) = \epsilon_d + t_1 \cos(k_x) + t_2 \cos(k_y)$, $\epsilon_{\text{top}} = \epsilon_s + dE$, and $\epsilon_{\text{bot}} = \epsilon_s - dE$.

After diagonalization of Eqs. (5) and (6), the FeSe monolayer's energy bands near the Fermi surface are plotted in Fig. 6, in which we have used the parameters of $\epsilon_d = 0.36$ eV, $\epsilon_s = -4.57$ eV, $d = 1.37$ Å, $t_1 = -0.01$ eV, $t_2 = 0.52$ eV and $t_3 = 0.71$ eV. The results show the Fermi surface distortion clearly. The energy bands are symmetric along X-M-X', and are the same for spin-up and spin-down electrons. In the presence of a nonzero vertical electric field, an energy splitting appears at M point. The amplitude of this splitting increases with increasing the electric field strength. The energy bands become asymmetric along X-M-X'. These features are quantitatively consistent with our DFT results [see Fig. (4)]. Thus, our tight-binding model further explains the origin of energy bands distortion in FeSe/SrTiO₃. Here, it should be noticed that in order to describe the electronic structures for the entire Brillouin zone, the tight-binding model should contain Fe d_{z^2} orbital besides the orbitals discussed above, since the energy band β in Fig. 2 at Γ point is mainly contributed by d_{z^2} orbital.

To summarize, by performing the *ab initio* calculations, we have systematically investigated the electronic structure of AFM FeSe monolayer on TiO₂ terminated SrTiO₃(001) surface. We have shown that the interaction between SrTiO₃(001) substrate and AFM FeSe monolayer induces charge transfer and a self-constructed electric field, which fundamentally modify the band structure and Fermi surface topology of the FeSe monolayer. In particular, the energy bands near the Fermi level are dramatically distorted by the electric field and show an obvious spin-resolved splitting around M point in BZ. As a result, the spin-resolved electron pockets evolved from band α become anisotropic and flat. We have proposed a tight-binding model Hamiltonian to reproduce these features. Also, we have shown that the present monolayer FeSe/SrTiO₃(001) composite structure is an ideal electron-hole bilayer system, with electrons and holes respectively formed in FeSe monolayer and TiO₂. These findings are to be verified by the future spin-polarized ARPES experiments and are expected to shed light on the high-temperature superconductivity or superfluidity at oxide interfaces.

Methods

The total energy and electronic structure calculations are performed by using projector augmented wave (PAW) method^{45–48}. The exchange correlation potential is described by the generalized gradient approximation (GGA) of Perdew-Burke-Ernzerhof (PBE) type⁴⁹. The plane wave cut-off energy is chosen to be 400 eV, which is converged in our test. $9 \times 9 \times 1$ and $6 \times 6 \times 1$ Monkhorst-Pack k -points are used in the reciprocal space integration for 1×1 and $\sqrt{2} \times \sqrt{2}$ supercells. The system is relaxed until the force on each atom is smaller than 0.01 eV/Å. To include the strong correlation effect for d electrons of Fe atoms, we adopt Hubbard- U correction. We use $U = 0.5$ eV for Fe-3d electrons in our main calculations, and the influence of different values of Hubbard- U on electronic structures are also discussed in the main text. All the DFT calculations are performed by using Vienna Ab-initio Simulation Package (VASP)⁴⁴.

- Hsu, F.-C. *et al.* Superconductivity in the PbO-type structure α -FeSe. *Proc. Natl. Acad. Sci. U.S.A.* **105**, 14262–14264 (2008).
- Wang, Q.-Y. *et al.* Interface-Induced High-Temperature Superconductivity in Single Unit-Cell FeSe Films on SrTiO₃. *Chin. Phys. Lett.* **29**, 037402 (2012).
- Liu, D.-F. *et al.* Electronic origin of high-temperature superconductivity in single-layer FeSe superconductor. *Nat. Commun.* **3**, 931 (2012).
- He, S.-L. *et al.* Phase diagram and high temperature superconductivity at 65 K in tuning carrier concentration of single-layer FeSe films. *Nat. Mater.* **12**, 605 (2013).
- Tan, S. Y. *et al.* Interface-induced superconductivity and strain-dependent spin density wave in FeSe/SrTiO₃ thin films. *Nat. Mater.* **12**, 634 (2013).
- Xiang, Y.-Y., Wang, F., Wang, D., Wang, Q.-H. & Lee, D.-H. High-temperature superconductivity at the FeSe/SrTiO₃ interface. *Phys. Rev. B* **86**, 134508 (2012).
- Hu, J. & Hao, N. S₄ Symmetric Microscopic Model for Iron-Based Superconductors. *Phys. Rev. X* **2**, 021009 (2012).
- Liu, K., Lu, Z.-Y. & Xiang, T. Atomic and electronic structures of FeSe monolayer and bilayer thin films on SrTiO₃(001): First-principles study. *Phys. Rev. B* **85**, 235123 (2012).
- Bazhiron, T. & Cohen, M. L. Effects of charge doping and constrained magnetization on the electronic structure of an FeSe monolayer. *J. Phys. Condens. Mater.* **25**, 105506 (2013).
- Bickel, N., Schmidt, G., Heinz, K. & Muller, K. Ferroelectric relaxation of the SrTiO₃(100) surface. *Phys. Rev. Lett.* **62** 2009 (1989).
- Heifets, E., Eglitis, R. I., Kotomin, E. A., Maier, J. & Borstel, G. Ab initio modeling of surface structure for SrTiO₃ perovskite crystals. *Phys. Rev. B* **64**, 235417 (2001).
- Heifets, E., Eglitis, R. I., Kotomin, E. A., Maier, J. & Borstel, G. First-principles calculations for SrTiO₃(100) surface structure. *Surf. Sci.* **513**, 211 (2002).
- Jauch, W. & Palmer, A. Anomalous zero-point motion in SrTiO₃: Results from -ray diffraction. *Phys. Rev. B* **60**, 2961 (1999).
- Kresse, G. & Furthmuller, J. Efficiency of ab-initio total energy calculations for metals and semiconductors using a plane-wave basis set. *Comp. Mater. Sci.* **6**, 15 (1996).
- Kresse, G. & Hafner, J. Ab initio molecular dynamics for liquid metals. *Phys. Rev. B* **47**, 558 (1993).
- Kresse, G. & Furthmuller, J. Efficient iterative schemes for ab initio total-energy calculations using a plane-wave basis set. *Phys. Rev. B* **54**, 11169 (1996).
- Bloch, P. E. Projector augmented-wave method. *Phys. Rev. B* **50**, 17953 (1994).
- Kresse, G. & Joubert, D. From ultrasoft pseudopotentials to the projector augmented-wave method. *Phys. Rev. B* **59**, 1758 (1999).
- Perdew, J. P., Burke, K. & Ernzerhof, M. Generalized gradient approximation made simple. *Phys. Rev. Lett.* **77**, 3865 (1996).

Acknowledgements

This work was supported by Natural Science Foundation of China under Grants No. 90921003 and No. 11004013, and by the National Basic Research Program of China (973 Program) under Grant No. 2009CB929103.

Author contributions

F.Z. and Z.W. did the calculations. P.Z., W.K., F.Z. and Z.W. analyzed the results. F.Z. and P.Z. wrote the paper. P.Z. was responsible for project planning and execution.

Additional information

Competing financial interests: The authors declare no competing financial interests.

How to cite this article: Zheng, F.W., Wang, Z.G., Kang, W. & Zhang, P. Antiferromagnetic FeSe monolayer on SrTiO₃: The charge doping and electric field effects. *Sci. Rep.* **3**, 2213; DOI:10.1038/srep02213 (2013).



This work is licensed under a Creative Commons Attribution-NonCommercial-NoDerivs 3.0 Unported license. To view a copy of this license, visit <http://creativecommons.org/licenses/by-nc-nd/3.0>